The Application of IT8.7/3 Test Target in Color Transformations for Printing Devices via Look-Up Tables

Mei-Chun Lo*, Yui-Liang Chen♦, Chia-Wei Chang *, Yu-Lin Chen*

Key words: printing characterization, color management system, color transformation, masking equation, linear model, polynomial regression, look-up tables, GCR, IT8.7/3, color image processing, spatial filtering, weighted-average filter, tetrahedral interpolation, SVD.

Abstract: In the application of color management system, color transformations between color imaging devices through the medium of CIE colorimetry, practically, use look-up tables, as they will normally be more computationally efficient than a physical mathematical basis. The aim of this study was, hence, to develop an image-processing algorithm efficiently to perform color transformations for printing devices via look-up tables (LUTs). Three processes of color transformation were implemented and evaluated. Those are: 1) scanner to printer, 2) monitor to printer, and 3) printer to monitor. Works subsequently accomplished include to:

1) Derived a well-performing printing characterization model carried out both forward (from colorant amounts) and also reverse transforms (into colorant amounts). This is the 2nd-order-SVD (singular-value decomposition) BPA applying polynomial regression, in terms of test target of IT8.7/3 produced using a printing device in interest;
2) Generated look-up tables (LUTs) using various different data-size approaches through refined models above;
3) Evaluated prediction performances of different LUT data-size approaches for each of 3 imaging devices used (monitor, scanner, and mainly printer);
4) Performed actual color transforms of complex images, using derived LUTs which gave reasonably prediction results, with tetrahedral interpolation. Additionally, a weighted-average spatial filtering method was implemented with convolution masks for noise removal.
5) Conducted advanced evaluations of models' performances using those complex images produced across media, via forced-choice paired-comparison psychological experiments.

Performances of characterization models derived were investigated using the corresponding training data set (in terms of ΔE of CIE94 or CIE2000). Also, the GCR (Gray component replacement) approach was carried out in reverse transforms of printing model to both reduce the use of three pigments in producing gray components and enhance the detail of shadow areas of reproductions.

---

* Dept. of Graphic Communications and Technology, Shih Hsin University, Taiwan, R.O.C.

♦ Dept. of Information Management, Shih Hsin University, Taiwan, R.O.C.

INTRODUCTION

Accurate color management across multiple imaging media is an important problem, and will become more important in years to come. In both of graphic arts industry and desktop publishing, in order to utilize color effectively, users are increasingly employing digital displays to create, view and present color images, or simulate the reproductions of presses/printers. The prediction of colors across various imaging devices requires implementation of several concepts, including device characterization, gamut mapping, and color appearance modeling. Due to computational efficiency, color transformations through the medium of CIE colorimetry, practically, are used look-up tables with interpolation approaches rather than on a mathematical basis.

This paper is focused on the concept of device characterization, mainly based on LUT approaches, to establish mappings between digital device-dependent values d_i (i=R,G,B or C,M,Y,K) and colorimetric values XYZ/L*a*b*. The LUT approaches were implemented using mathematical characterization models well-derived previously for imaging devices considered. Three types of imaging media were tested, including a RGB format of scanner, a CMYK four-color printer, and a HDTV CRT monitor. The printing device was primarily in interest, and characterized using the IT8.7/3 test target.

There are several well-known types of characterization models that colorimetrically carry out both forward (from device-dependent data) and reverse transform (into device-dependent values). Three of which were implemented in this experiment: 3D or 4D Lookup Table (LUT) of tetrahedral interpolation (Hung 1993), linear model and masking model. The LUT method uses a pair of three-dimensional or four-dimensional tables to associate a triplet of L*a*b* with every RGB or CMYK combination respectively, and vice versa.

The term *linear model* refers to the PLCC model (Luo et al. 1991) that predict tristimulus response with a linear combination of pure phosphor output for the CRT monitor. The PLCC model starts by linearizing each of RGB digital input response curves with the specific nonlinear function from which they draw their names. The linear model has been widely used for CRT monitors, but may not apply on LCD displays, due to its assumption of channel independence.

The third type implemented was the masking model that applies polynomial regression with SVD (singular-value decomposition) approach (Press et al. 1993). Both of the 2nd-order-SVD BPA and the 3rd-order-SVD (Lo et al. 1998; Lo et al. 1999) models were used for the printing and the scanner devices considered respectively. The reverse transformation of printing model, applying the concept of GCR (gray component replacement) in a BPG (black printer generation) algorithm, masks inputs from 3-dimentional L*a*b* space to

4-dimensional CMYK space.

Additionally, for the removal of noises produced on digital images due to the LUT-based interpolation, one type of spatial filtering operations was implemented with a convolution mask. This was a weighted-average filtering method performed in the spatial domain (Efford 2000)

IMPLEMENTATION

Device Characterization

As mentioned above, in addition of a 4-color CMYK Epson printer, a Barco monitor and a RGB format of Acer 620PT scanner were tested in this study. All reflectance data, obtained from test targets of both IT8.7/3 and IT8.7/2 (ANSI 1993) for the printer and the scanner tested respectively, were collected using a Gretag Macbeth Spectrolino (spectrophotometer) across the visible spectrum (380-730nm) at 10-nanometer intervals. Then colorimetric data including CIE XYZ, CIE LAB, and CIE LCH were calculated for CIE illuminant D_{50} and the CIE 1931 standard observers. Then, both of the scanner and the printer considered used the masking type of device characterization models. A forward 3rd-order-SVD (singular-value decomposition) model (Lo et al. 1999), implementing using lightness-division strategy, was applied in the scanner; whereas both the forward and the reverse transforms of a 2nd-order-SVD BPA model which is based on the GCR concept were used for the printer (Lo et al. 1998). These two masking models all applied polynomial regression with SVD approach (Press et al. 1992).

The 2nd-order-SVD BPA model assumes that both three-color and black components are two separate parts in a four-color printing. Basically, this model is similar to the 2nd-order masking algorithm in the three-color reproduction described by Yule (1967) to apply all possible cross-terms. In this case, 27 terms were used to include all possible combinations of $(D_r, D_g, D_b)_{4c}$ and $(D_r, D_g, D_b)_k$. The forward and the reverse algorithms are given in Eqns. 1 and 2.

$$\begin{aligned} D_{r\text{-}4c} = {} & a_{1,1}D_{r\text{-}3c} + a_{1,2}D_{g\text{-}3c} + a_{1,3}D_{b\text{-}3c} + a_{1,4}D_{r\text{-}k} + a_{1,5}D_{g\text{-}k} + a_{1,6}D_{b\text{-}k} + \\ & a_{1,7}D^2_{r\text{-}3c} + a_{1,8}D^2_{g\text{-}3c} + a_{1,9}D^2_{b\text{-}3c} + a_{1,10}D^2_{r\text{-}k} + a_{1,11}D^2_{g\text{-}k} + a_{1,12}D^2_{b\text{-}k} + \\ & a_{1,13}D_{r\text{-}3c}D_{g\text{-}3c} + a_{1,14}D_{r\text{-}3c}D_{b\text{-}3c} + a_{1,15}D_{r\text{-}3c}D_{r\text{-}k} + a_{1,16}D_{r\text{-}3c}D_{g\text{-}k} + \\ & a_{1,17}D_{r\text{-}3c}D_{b\text{-}k} + a_{1,18}D_{g\text{-}3c}D_{b\text{-}3c} + a_{1,19}D_{g\text{-}3c}D_{r\text{-}k} + a_{1,20}D_{g\text{-}3c}D_{g\text{-}k} + \\ & a_{1,21}D_{g\text{-}3c}D_{b\text{-}k} + a_{1,22}D_{b\text{-}3c}D_{r\text{-}k} + a_{1,23}D_{b\text{-}3c}D_{g\text{-}k} + a_{1,24}D_{b\text{-}3c}D_{b\text{-}k} + \\ & a_{1,25}D_{r\text{-}k}D_{g\text{-}k} + a_{1,26}D_{r\text{-}k}D_{b\text{-}k} + a_{1,27}D_{g\text{-}k}D_{b\text{-}k} \end{aligned} \quad (1)$$

Similar terms are used for the calculation of $D_{g\text{-}4c}$ and $D_{b\text{-}4c}$.

$$
\begin{aligned}
D_{r\text{-}3c} = {} & b_{1,1}D_{r\text{-}4c} + b_{1,2}D_{g\text{-}4c} + b_{1,3}D_{b\text{-}4c} + b_{1,4}D_{r\text{-}k} + b_{1,5}D_{g\text{-}k} + b_{1,6}D_{b\text{-}k} + \\
& b_{1,7}D^2_{r\text{-}4c} + b_{1,8}D^2_{g\text{-}4c} + b_{1,9}D^2_{b\text{-}4c} + b_{1,10}D^2_{r\text{-}k} + b_{1,11}D^2_{g\text{-}k} + b_{1,12}D^2_{b\text{-}k} + \\
& b_{1,13}D_{r\text{-}4c}D_{g\text{-}4c} + b_{1,14}D_{r\text{-}4c}D_{b\text{-}4c} + b_{1,15}D_{r\text{-}4c}D_{r\text{-}k} + b_{1,16}D_{r\text{-}4c}D_{g\text{-}k} + \\
& b_{1,17}D_{r\text{-}4c}D_{b\text{-}k} + b_{1,18}D_{g\text{-}4c}D_{b\text{-}4c} + b_{1,19}D_{g\text{-}4c}D_{r\text{-}k} + b_{1,20}D_{g\text{-}4c}D_{g\text{-}k} + \\
& b_{1,21}D_{g\text{-}4c}D_{b\text{-}k} + b_{1,22}D_{b\text{-}4c}D_{r\text{-}k} + b_{1,23}D_{b\text{-}4c}D_{g\text{-}k} + b_{1,24}D_{b\text{-}4c}D_{b\text{-}k} + \\
& b_{1,25}D_{r\text{-}k}D_{g\text{-}k} + b_{1,26}D_{r\text{-}k}D_{b\text{-}k} + b_{1,27}D_{g\text{-}k}D_{b\text{-}k}
\end{aligned}
\tag{2}
$$

Similar terms are used for the calculation of $D_{g\text{-}3c}$ and $D_{b\text{-}3c}$.

Where ($D_{r\text{-}4c}$, $D_{g\text{-}4c}$, $D_{b\text{-}4c}$), ($D_{r\text{-}3c}$, $D_{g\text{-}3c}$, $D_{b\text{-}3c}$), ($D_{r\text{-}k}$, $D_{g\text{-}k}$, $D_{b\text{-}k}$) terms are the red-, green-, and blue- colorimetric densities of four-color, three-color component, and black component respectively.

The 3rd-order masking equations (Yule 1967) in both forms of the forward and the reverse were also used in the 2nd-order-SVD BPA model. It relates the 3-color components ($D_{r\text{-}3c}$, $D_{g\text{-}3c}$, $D_{b\text{-}3c}$) and (i.e. amounts (c, m, y) of three process color ink CMY. Here only the forward 3rd-order masking equations are given as follows,

$$
\begin{aligned}
D_{r\text{-}3c} = {} & a_{1,1}c + a_{1,2}m + a_{1,3}y + a_{1,4}c^2 + a_{1,5}m^2 + \\
& a_{1,6}y^2 + a_{1,7}cm + a_{1,8}cy + a_{1,9}my + a_{1,10}c^3 + \\
& a_{1,11}m^3 + a_{1,12}y^3 + a_{1,13}c^2m + a_{1,14}c^2y + a_{1,15}m^2c + \\
& a_{1,16}m^2y + a_{1,17}y^2c + a_{1,18}y^2m + a_{1,19}cmy
\end{aligned}
\tag{3}
$$

Similar terms are used for the calculation of $D_{g\text{-}3c}$ and $D_{b\text{-}3c}$.

Here c, m, y values (i.e. $D_{r\text{-}c}$, $D_{g\text{-}m}$, $D_{b\text{-}y}$ respectively) are the principal colorimetric densities which obtain by establishing a 1-D LUT between digital fractional dot areas (FDA) and colorimetric density on paper for each of three primaries CMY. They were normalized into 0.0 to 1.0 in this study. The colorimetric densities D_r, D_g, D_b and c, m, y are given by:

$$
\begin{aligned}
D_r &= \log (X_o / X) \\
D_g &= \log (Y_o / Y) \\
D_b &= \log (Z_o / Z)
\end{aligned}
\tag{4}
$$

$$
\begin{aligned}
c &= D_{r\text{-}c} = \log (X_o / X_c) \\
m &= D_{g\text{-}m} = \log (X_o / X_m) \\
y &= D_{b\text{-}y} = \log (X_o / X_y)
\end{aligned}
\tag{5}
$$

Where, (D_r, D_g, D_b) and (X, Y, Z) are the red-, green-, and blue- colorimetric densities and tristimulus values of a color stimulus in interest respectively. X_0, Y_0, and Z_0 — the tristimulus values of the paper substrate (white); (X_c, Y_m, and Z_y) — X value for the cyan, Y value for the magenta, and Z value for the yellow tints (halftone) respectively.

A Barco monitor internally set to CIE illuminant D_{50}, displayed colors or images in a dark room. A Photo Research SpectraScan 650 Spectrophometer was applied for the CRT data collection in a dark room at a fixed distance, perpendicular to the center of the display surface. Two suites of data were collected for the monitor: a 54-samples training data set, used in the derivation of the PLCC linear model, made up of 18 perceptually evenly spaced measurements for each primary RGB channel in terms of 15 DACs intervals; and a 9x9x9 grid, used for testing and verification, of evenly spaced RGB values covering the entire 3D space.

It was found that performances of mathematical DC Models derived were 1.58, 0.62, and 1.49 of the mean CIE94 ΔE values for the scanner, the monitor and the printer respectively. Apparently, from results evaluated, all 3 mathematical DC models for these 3 imaging devices mentioned above, gave satisfactory or reasonably predictions.

3D Lookup Tables

The 3D lookup table (LUT) (i.e. $n_1 \times n_2 \times n_3$; n_1, n_2, n_3 are the number of levels along each corresponding axis of the color space considered) with interpolation has become a relatively practical development in color space transformation. Actually, a 3-color imaging system (such as. the monitor and the scanner tested here), can use only one suite of 3D LUT method in interpolation; but a 4-color CMYK printing system with the GCR application, then, needs a few suits of LUTs in terms of various black ink levels ranging from 0 to 100 (i.e. uses a 4-D LUT method). The n_4 denotes K axis or channel in this study. The matrix of $n_1 \times n_2 \times n_3$ or $n_1 \times n_2 \times n_3 \times n_4$ corresponding values at lattice points for each of the source (input) and the destination (output) spaces were tabulated into lookup table using the respective 3-color or 4-color system's linear or masking model well-derived earlier. The 3D LUT method was implemented with the intention of providing a practical standard, also against which to evaluate its respective linear or masking mathematical model derived. Here, both the forward and the reverse LUTs were produced for both the monitor and the printer; while only the forward LUT for the scanner. At look-up time for color space transformation, the 3D tetrahedral interpolation was used to look up or predict corresponding values. Tetrahedral Interpolation was chosen over a number of other methods primarily for its speed and ability to handle sparse, irregularly spaced data (Hung 1993).

Gamut Mapping

However, any values that fall outside the convex hull of the measured or predicted gamut would return errors. This is particularly problematic for the printers, which have slightly convex gamut faces (see Figure 1). In order to prevent edge values from returning invalid data, the entire lookup table was tabulated by applying a gamut-mapping algorithm (GMA) using the clipping method with a Single focal point of L* = 50, in addition of the corresponding linear or masking model derived (Lo et al. 2003). However, a lightness (L*) mapping was previously carried out before the clipping method in transformation of color data across media to enhance or optimally retain detail-rendition.

Four categories of lightness-mapping approaches were derived here. Either of both expansion and compression of the dynamic range of L* Channel in both of highlight and shadow areas, would be applied accordingly for each imaging device considered. The details of the derivation of those approaches are explained as follows (Figures 1 to 4).

1. Optimally retain details of shadow area in the reverse mapping

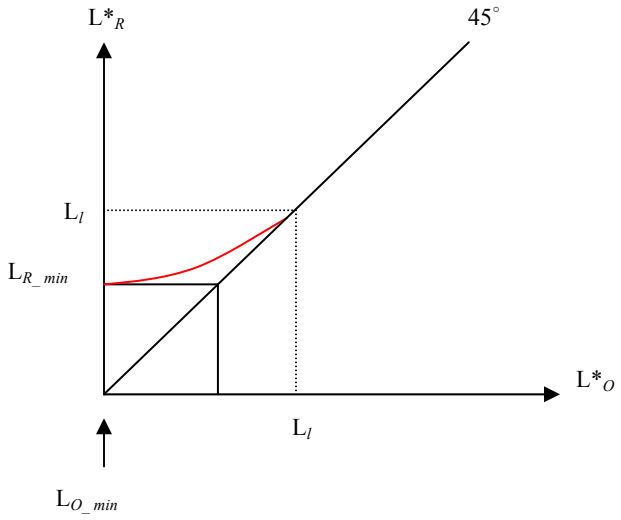

Figure 1 Optimally retain details of shadow area in reverse mapping (if $L_O < L_{O\_min}$, then adjust => $L_O = L_{O\_min}$).

The L* channel in shadow area is compressed across media when the minimal L* value for destination device (i.e. Reproduction, *R*) is larger than that for source device (i.e. Original, *O*). This approach is used in the reverse mapping, wherein: $L_O{}^*a_O{}^*b_O{}^* \rightarrow L_R{}^*a_R{}^*b_R{}^*$compressed$\rightarrow R_RG_RB_R$ or $C_RM_RY_R/C_RM_RY_RK_R$ (see Figure 1).

The compression approach for shadow area:

$$(L_l - L_O)^r = L_l - L_R$$

$$\Rightarrow \quad L_R = L_l - (L_l - L_O)^r$$

$$\Rightarrow \quad \because L_O = L_{O\_min} = 0, \text{ and } L_R = L_{R\_min}$$

$$\Rightarrow \quad L_l^r = L_l - L_{R\_min}$$

$$\Rightarrow \quad r \times \log (L_l - L_{O\_min}) = \log (L_l - L_{R\_min})$$

$$\Rightarrow \quad r = \frac{\log(L_l - L_{R\_\min})}{\log(L_l - L_{O\_\min})}$$

$$\Rightarrow \quad \because \text{Normally } L_{O\_min} = 0 \ \therefore \ r = \frac{\log(L_l - L_{R\_\min})}{\log L_l}$$

Where L_R, output L* ; L_O, input; L_l, L* for start point of compression; L_{O_min}, minimum L*of source devic; L_{R_min} , minimum L* of destination device.

2. Enhance details of shadow area in the forward mapping

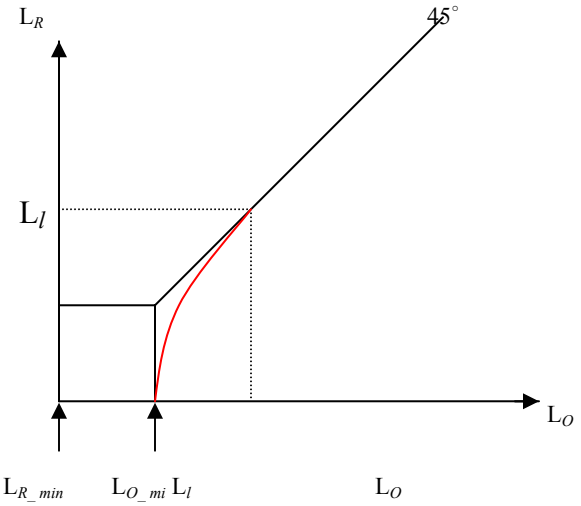

Figure 2 Enhance details of shadow area in forward mapping (if $L_O < L_{O\_min,}$ then adjust => $L_O = L_{O\_min}$).

The L* channel in shadow area is extended across media when the minimal L* value for destination (i.e. Reproduction, *R*) device is less than that for source device. This approach is used in the forward mapping, wherein: $R_OG_OB_O$ or $C_OM_OY_O/C_OM_OY_OK_O \rightarrow L_O{*}a_O{*}b_O{*} \rightarrow L_R{*}a_R{*}b_R$ extended (see Figure 2).

The extension approach for shadow area:

$$\Rightarrow \quad (L_l - L_R)^r = L_l - L_O$$

$$\Rightarrow \quad r \times \log (L_I - L_R) = \log (L_I - L_O)$$

$$\because L_O = L_{O\_min}, \text{ and } L_R = L_{R\_min} = 0$$

$$\Rightarrow \quad r = \frac{\log(L_I - L_{O\_min})}{\log(L_I - L_{R\_min})}$$

$$\Rightarrow \quad r = \frac{\log(L_I - L_{O\_min})}{\log L_I}$$

$$\Rightarrow \quad \log (L_I - L_R) = \frac{\log(L_I - L_O)}{r}$$

$$\Rightarrow \quad L_I - L_R = 10^{(\log(L_I - L_O)/r)}$$

$$\Rightarrow \quad = (10^{\log(L_I - L_O)})^{1/r}$$

$$\Rightarrow \quad = (L_I - L_O)^{1/r}$$

$$\Rightarrow \quad L_R = L_I - (L_I - L_O)^{1/r}$$

Where L_R, output L*; L_O, input L*; L_h, L* for start point of extension; L_{O_max}, original maximum L* of source device; L_{R_max}, maximum L* modified for source device before connected with destination device.

3. Optimally retain details of highlight area in the reverse mapping

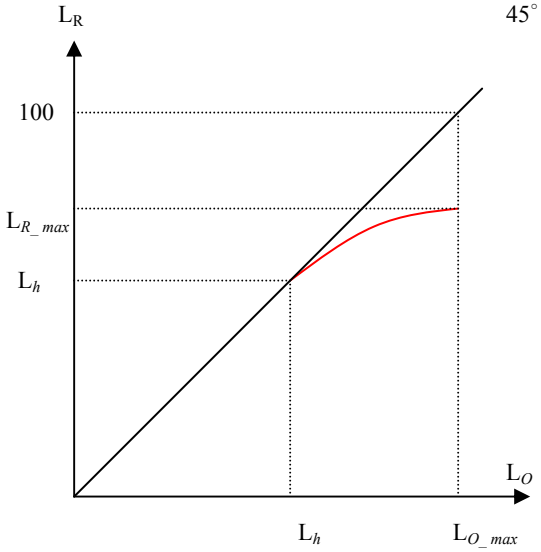

Figure 3 Optimally retain details of highlight area in the reverse mapping (if $L_O > L_{O\_max}$, then adjust $\Rightarrow$ $L_O = L_{O\_max}$)

The L* channel in highlight area is compressed across media when the maximal L* value for destination device is less than that for source device. This approach is used in the reverse mapping, wherein: L*a*b*→L*a*b*compressed →RGB or CMY/CMYK (see Figure 3).

The compression approach for highlight area:

$\Rightarrow \quad (L_R - L_h)=(L_O - L_h)^{r}$

$\Rightarrow \quad L_R = (L_O - L_h)^{r} + L_h$

$\Rightarrow \quad \because L_O = L_{O\_max}$, and $L_R = L_{R\_max}$

$\Rightarrow \quad \therefore L_{R\_max} - L_h = (L_{O\_max} - L_h)^{r}$

$\Rightarrow \quad \log (L_{R\_max} - L_h) = r \times \log (L_{O\_max} - L_h)$

$\Rightarrow \quad r = \dfrac{\log(L_{R\_max} - L_h)}{\log(L_{O\_max} - L_h)}$

Where L_R, output L*; L_O: input); L_h , L* for start point of compression; L_{R_max}, maximum L*of destination device; L_{O_max}, maximum L*of source device.

4. Enhance details of highlight area in the forward mapping

The L* channel in highlight area is extended across media when the maximal L* value for destination device is larger than that for source device. This approach is used in the forward mapping, wherein: RGB or CMY/CMYK →L*a*b*→L*a*b* extended (see Figure 4).

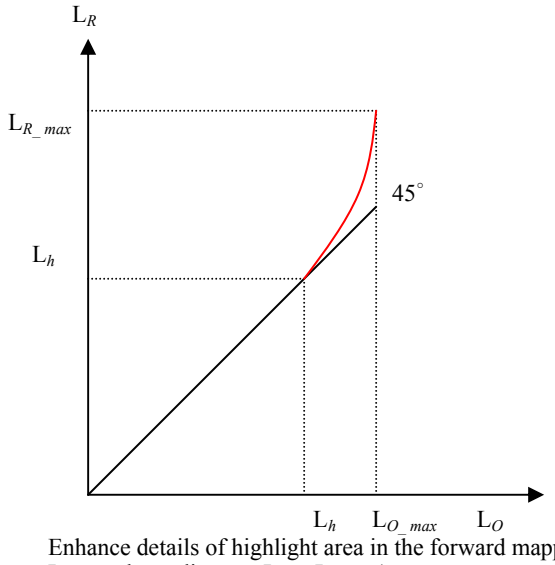

Figure 4 Enhance details of highlight area in the forward mapping (If $L_O < L_{O\_max}$, then adjust => $L_O = L_{O\_max}$)

The extension approach for highlight area:

$$\Rightarrow \quad (L_O - L_h) = (L_R - L_h)^{r}$$

$$\Rightarrow \quad r \times \log (L_R - L_h) = \log (L_O - L_h)$$

$$\Rightarrow \quad r = \frac{\log(L_O - L_h)}{\log(L_R - L_h)}$$

$$\Rightarrow \quad \because L_o = L_{o\_max}, \text{ and } L_R = L_{R\_max} = 100$$

$$\Rightarrow \quad \therefore r = \frac{\log(L_{O\_max} - L_h)}{\log(L_{R\_max} - L_h)}$$

$$\Rightarrow \quad \log (L_R - L_h) = \frac{\log(L_O - L_h)}{r}$$

$$\Rightarrow \quad \text{Normally } L_{R\_max} = 100$$

$$\Rightarrow \quad (L_R - L_h) = 10^{\log(L_O - L_h)/r}$$

$$\Rightarrow \quad = (10^{\log(L_O - L_h)})^{1/r}$$

$$\Rightarrow \quad = (L_O - L_h)^{1/r}$$

$$\Rightarrow \quad L_R = (L_O - L_h)^{1/r} + L_h$$

$$\Rightarrow \quad L_R = L_h + (L_O - L_h)^{1/r}$$

Where L_R, output L*；L_O: input L*; L_h, L* for start point of extension ;L_{O_max}, original L* maximum of source device; L_{R_max}, L* maximum modified for source device before connected with destination device.

Spatial Filtering

As mentioned earlier, the LUT method has been practically used in the color image transformation across imaging devices. The aim of this study is, hence, to develop an image-processing algorithm efficiently to perform color transformations (but mainly in interest for printing devices) via look-up tables (LUTs). However the LUTs created in this study were tabulated using the linear or masking characterization models derived. The prediction errors of reproduction images obtained from these LUT transform method were larger than those obtained using respectively mathematical linear or masking models. Therefore, a weighted-average filtering method was also derived in this study (Efford 2000). It reconstructed reproduction images of both the printing halftone and the screenless monitor after performing cross-media color transformation via LUTs.

EXPERIMENTAL PREPARATIONS

Image Preparation and Processing

As mentioned previously, the printer characterization was the focus of this

research in the color transformation across media. Therefore the computational procedures for the 4-color printing process would be given in more details here. Both of the forward and the reverse 2nd-order-SVD BPA models of a masking type were implemented for the printer device tested. Figures 5 and 6 show the computational procedures for both forward and reverse mappings respectively.

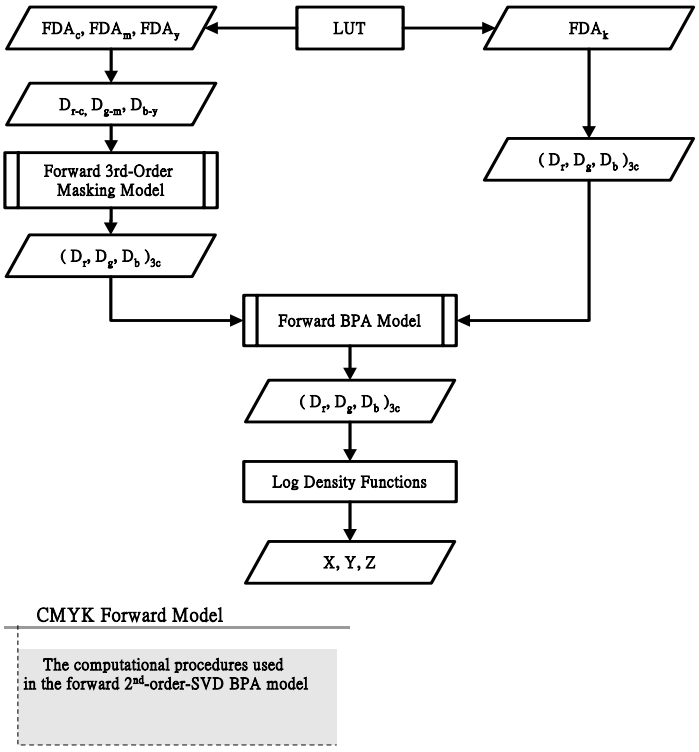

Figure 5 Schematic diagram of computational procedures used in the masking type of forward 2nd-order SVD BPA model for the 4-color CMYK printing process tested.

Both the forward and the reverse computational procedures are revised from those in CMYKRG 7-color printing process developed earlier (Lo et al. 1997). All the same parameters are used here.

Cross-Media Color Transformation Processes

Three color imaging devices were tested, including a scanner, a monitor, and a printer. Therefore, three processes of color transforms across media were decided in this study. Those are scanner-to-printer, monitor-to-printer, and printer-to-monitor. These 3 processes are detailed in Figure 7.

Approaches of Created LUT Data Size

When creating the lookup table, a decision must be made regarding the size of the training data set. In general, a larger training set is better, but the benefit tapers off after some certain data points. Initially a few suits of LUT, with different data sizes, were created for each of 3 imaging devices for either of forward or reverse color-space mappings; and tested their prediction performances. Then, the optimal LUT lattice points, used for imaging devices considered, were decided to ensure reasonably minimal error introduced by the known training data-size. Decidedly, LUTs with lattice-points (i.e. n1×n2×n3) of 52x52x52 and 21x65x65, both having optimal performances (i.e. reasonably minimal errors introduced by the known training data-size), were chosen for both the monitor and the scanner in the forward mapping; and for the monitor in the reverse mapping, respectively. As for the printer, three different data sizes of LUT (denoted as Regular, Dynamic 1, and Dynamic 2 in Table 1), were applied for both the forward and the reverse mappings, used in the application of cross-media color transforms for complex images. One (denoted as Regular) was regular-grids (i.e. even spaced), and the other two dynamic-grids (i.e. irregular spaced) LUTs, Both the Dynamic1 and the Dynamic2 LUTs, used for both forward and reverse mappings, had denser points in areas of the highlight to middle tone than those in the shadow area. But Dynamic2's LUT data size was larger, especially more lattice points in a*b* channels, than Dynamic1's.

Table 1 Three different lattice points of LUTs, used for both of forward and reverse color mappings generated for the 4-color printer device.

Color Space	Data Size (n1× n2 × n3× n4)		
	Dynamic 1	Dynamic 2	Regular
CMYK (Forward)	22×22×22×22	24×24×24×24	21×21×21×21
L*a*b* and K (Reverse)	18×55×55×22	22×65×65×24	21×65×65×21

Images

Test images used were categorized into two types according to both the input and the output devices used in the color transform. A shown in Plate 1, the former five images were used for the scanner-to-printer process, whereas the latter five digital sRGB (ISO/DIS 2000) images were used for both processes of the printer-to-monitor and the monitor-to-printer. Overall, thus, 10 images were tested.

Totally, combined 3 different data sizes of LUT approaches *with* or *without* the filtering method mentioned earlier, every process implemented 6 color transforms (i.e. 6 reproduction images) of every complex image considered.

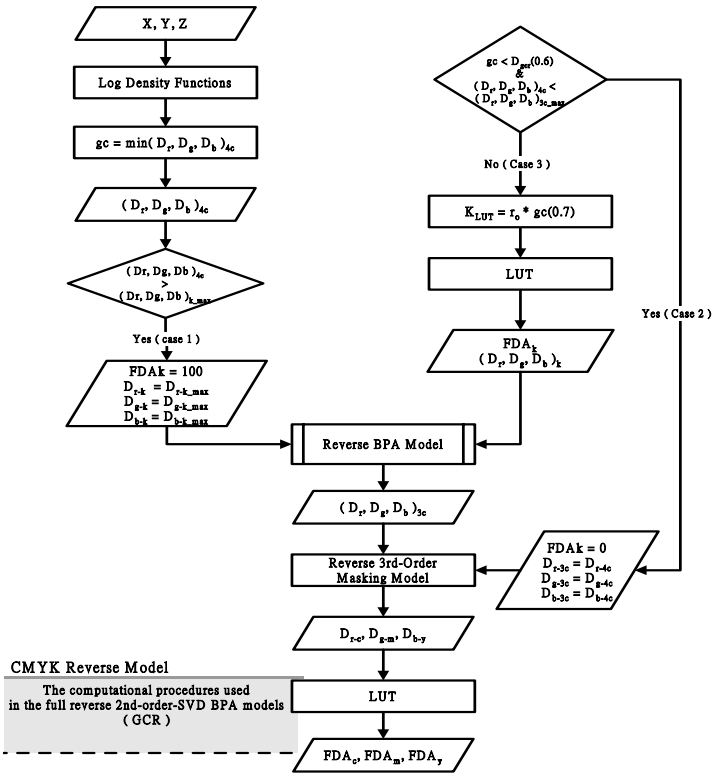

Figure 6 Schematic diagram of computational procedures used in the masking type of reverse 2nd-order-SVD BPA model for the 4-color CMYK process tested.

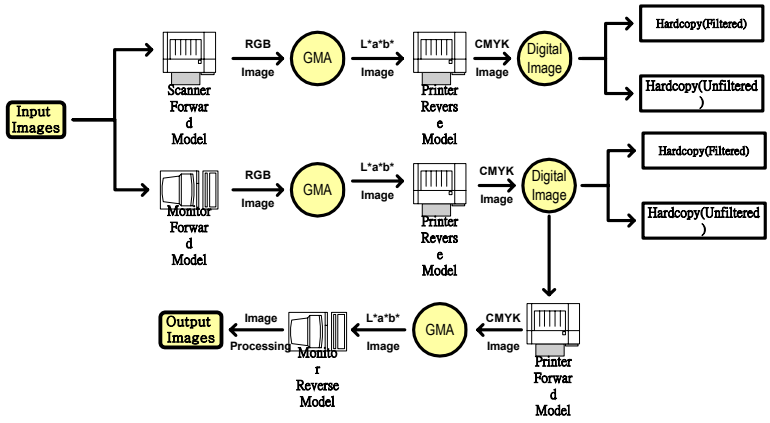

Figure 7 Three processes of color transforms for scanner-to-printer, monitor-to-printer, and printer-to-monitor used in the study.

EXPERIMENTS

Viewing Configurations and Conditions

The sRGB monitor's white point was set to the chromaticity near the CIE Illuminant D_{65} with a peak luminance of 80 cd/m^2. The original or reproduced images were viewed in a light booth with the same color temperature and peak luminance as sRGB monitor's setting, under a dark viewing surround. For color-rendition evaluations of the scanner-to-printer transformation, the original photographs and the corresponding printed hardcopies were viewed in a light booth as the same setting described above.

Viewing Technique

Psychophysical experiments had been conducted to make comparisons of color appearance matching between the original images (sRGB monitor images or photographs) and the printed images (reproduced via cross-media color transforms). A forced-choice paired comparison method, with simultaneously binocular viewing technique, was employed in this experiment.

As mentioned earlier, three categories of color-transform processes were evaluated here. These processes include 1) the scanner to printer; 2) the monitor to printer; and 3) the printer to monitor. Therefore three types of paired-comparison were carried out in this study, including 1) photograph to printed reproduction; 2) original monitor image to printed reproduction; and 3) printed original to reproduced monitor image. The 3 LUT models mentioned previously were tested for each of 3 cross-media color transform processes.

Two stages of experiments were conducted. In the first stage, the judgement was based on the color-fidelity quality for test images reproduced by the 3 data-size approaches of LUTs derived, without spatial filtering used, in every cross-media color transform process in interest. Then comparisons would be further made between pictures produced *with* and *without* the spatial filtering, using the best performing LUT model found in the first stage. A panel of 10 observers, repeatedly twice, viewed a paired of reproductions, to judge which of the two gave a better match on color fidelity of an original considered.

DATA ANALYSIS

The resulted visual data were analyzed using the laws of comparative judgment (Thurstone 1927, Bartleson and Grum 1984). Therefore a series of interval scales (mean Z score values) were generated that defined both the ranking order of algorithms performances and a gauge of the relative difference between techniques in interest.

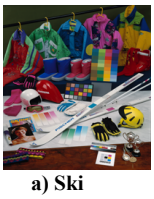

a) Ski

b) Color Rendition Chart

c) Bride

d) Fruits

e) Shoot

f) Kids

g) GATF 7090-13

h) Women

i) Magic

Plate 1 Test images used in the evaluation of color transforms for the scanner-to-printer (using (a) to (e)) and both of the printer-to-monitor and the monitor-to-printer (using (f) to (j)).

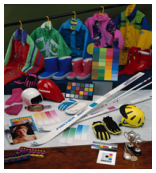

j) Ski

A higher value indicates that a better matching is obtained between the reproduced image after color-transform mapping considered and the corresponding original image. Complementarily the mean scale values of category for each of 3 LUT models tested would be averaged from the visual raw data accessed using the categorical method for each of 3 color-transform processes in question. Those were used to identify models' categorical ranking in color fidelity.

RESULTS AND DISCUSSIONS

Device Characterization

Three data sizes of LUTs were created using the printing device models derived. The prediction results (in terms of mean ΔE CIE2000) are tabulated in Table 2. All these LUT models were further, implemented, with/without the filtering method mentioned earlier, in the cross-media color transform for color complex images.

It can be seen that both models of the Dynamic 1 and the Dynamic 2 had better predictions than the Regular model for both the forward and the reverse mapping transform. However, there was a very little difference of performances between the Dynamic 1 and the Dynamic 2, but with the latter performing a slightly better. It implies that LUT should have denser lattice-points in the

highlight to middle tone areas than those in the shadow areas; also, a LUT with larger data size performed better than those with smaller data size.

Table 2 Comparisons of Mean ΔE CIE2000 of LUTs models with 3 different 4D lattice-points combinations in both 1) the color space of C, M, Y and K for the forward mapping, and 2) the color space of L, a*, b* and K for the reverse mapping, for the printer device tested.

Mapping \ Models	Dynamic 1	Dynamic 2	Regular
Forward (CMYK Color Space)	4.94	4.67	6.36
Reverse (L*a*b* and K Color Space)	6.79	6.45	7.19

Psychological Experiments

The results, in terms of z-score obtained using the law of comparative judgment, are summarized in Tables 3(a) to 3(c), for color transforms of the scanner-to-printer, the monitor-to-printer, and the printer-to-monitor respectively. The overall results are also depicted in Figures 8(a) to 8(c). The ordinate shows the interval psychophysical scales (*Z* scores) calculated statistically from the experimental data. The abscissa represents the models of interest, and each line drawn (error bar) indicates the 95% confidence limit (CL) of the corresponding model (Lo et al. 1996). A model evaluated is considered not to be significantly different from another if its mean z score is within the 95% confidence limit (CL, i.e. ±2 units of standard deviations) of the other. Hence, these two models would be ranked in the same order.

The results, obtained from overall images, showed that the rank of 3 LUT models performance (here without filtering) for each process of color transforms reasonably accorded with the one found in the evaluation of test/training data sets. Those 2 Dynamic LUT models outperformed the Regular models for all 3 color-transform processes, for both the forward and reverse mappings. Additionally, both of the Dynamic models had similar prediction performances in all phases, except in the scanner-to-printer transform wherein the Dynamic 2 performed much better than the Dynamic 1. Also, From further stage of comparisons results obtained between with and without using the spatial filtering, it clearly showed, overall, any phase of model with filtering always gave a better prediction than the same phase one but without filtering. Especially, from the analysis of results obtained from each single image, it strongly showed that some pictures (e.g. having with skin tone colors) had a much better rendition by using filtering. However, it was also found insignificantly differences of color-rendition quality, between reproductions using with/without filtering, for some test images.

Table 3 Paired-comparison results in terms of z-score scale, based on the judgments made for the overall color-fidelity accuracy of every image and all 5 test images combined, for every cross-media color transform of a) the scanner-to-printer, b) the monitor-to-printer, and c) the printer-to-monitor. (95% CL = ±1.07 for each image, 95% CL = ±0.4382 for overall images)

(a) Z-score value obtained from the color transform of scanner to printer.

	Dynamic 1	Dynamic 2	Regular
Ski	-0.22	1.09	-0.87
Color Rendition Chart	-0.94	1.05	-0.10
Bride	0.05	0.97	-1.02
Fruits	0.52	0.63	-1.15
Shoot	-0.10	1.05	-0.94
Overall (Mean)	-0.17	1.07	-0.90

(b) Z-score obtained from the color transform of monitor-to-printer

	Dynamic 1	Dynamic 2	Regular
Ski	0.94	0.10	-1.04
Color Rendition Chart	0.83	0.28	-1.11
Bride	0.55	0.61	-1.15
Fruits	0.34	0.79	-1.13
Shoot	0.10	0.94	-1.05
Overall (Mean)	0.57	0.58	-1.15

(c) Z-score value obtained from the color transform of printer-to-monitor

	Dynamic 1	Dynamic 2	Regular
Ski	0.93	0.12	-1.05
Color Rendition Chart	0.48	0.67	-1.15
Bride	0.76	0.38	-1.13
Fruits	0.74	0.40	-1.14
Shoot	-0.11	1.05	-0.94
Overall (Mean)	0.57	0.58	-1.15

Note: 1) "F" means *with filtering* "NF" means "*without filtering*"; D1, D2 ,and R represent those LUT data-size approaches of, the *Dynamic 1*, *Dynamic 2* ,and the *Regular* respectively, shown in Table 1); 2) The underlined figure indicates the best performing model for a particular image or overall images, and CL represents confidence limit

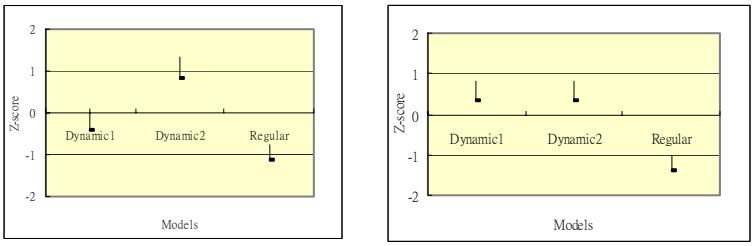

(a) Scanner-to-Printer (b) Printer-to-Monitor

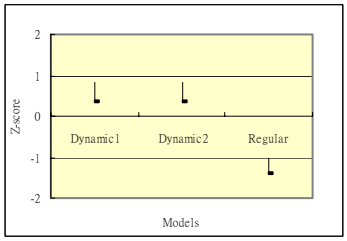

(c)Monitor-to-Printer

Figure 8 Different models' performance for the overall color–fidelity accuracy of all the 5 tested images for color transforms of (a) the scanner-to-printer, (b) the printer-to-monitor, (b) the monitor-to-printer (including 95% confidence limit).

CONCLUSIONS

This paper proposed both 3-D and 4-D LUT methods in the application of cross-media color transformations for complex images. The 3-D or 4-D LUT method proposed was created, in terms of training data sets commonly on standardized test target, using practically mathematical approach of device characterization models. Printing devices were mainly concerned in this study. Another two imaging devices, a scanner and a monitor were also used here for the application of color transformation *from or to* the printing device tested. The international standardized IT8.7/3 target was applied for the printing device. Due to a fixed size of training data sets on test target, a few suits of LUTs with different data sizes, for each of imaging devices were produced and investigated to decide the optimal LUT lattice points for the known size of target training sets. Preliminarily, three devices models were evaluated with different approaches of LUT data sizes. Only the best performing approach found for each of the scanner and the monitor was further implemented in the color transformation for complex images across media linking with printing device tested in this study. As for the printing device, three well performing approaches were chosen to carry out in the cross-media color transformation of complex images.

Conclusively, a use of spatial filtering was suggested here to reduce the noise effect produced from those 3D or 4D LUTs created using mathematical models.

However form the results obtained, it also showed the properties of an image could vary spatially; thus, the derived filtering method that performed well in one part of an image was not guaranteed to perform well in another part of this image. It applies that an adaptive filtering method should be adopted, to optimally set values of the *outlier* (i.e. the coefficient of variation) according to characteristics of the images in question.

Overall, LUTs, in both color spaces of the CMYK and the L*a*b* and K* respectively for both the forward and the reverse mappings, should have denser lattice-points in the highlight to middle tone areas than those in the shadow areas. Also reasonably, LUTs with larger data-size gave better predictions performance than those with smaller data-size.

The further works are: 1)to derive heuristically performing-well adaptive filtering methods, e.g. MMSE (Efford 2000), and also to automatically decide the optimal outlier for the coefficient of variation; 2) revise the element- category arrangement in the IT8.7/3 test target based on results obtained from the investigation of models performance, using the training data set (e.g. to include some more data sets in skin tones); 3) Refine and modify the 2^{nd}-order-SVD BPA printing characterization models using lightness-division approach and the revised IT8.7/3 test target; 4) also refine the spectral cellular Neugebauer model derived earlier, then further implement into LUT method to apply in cross-media color transformation for complex images, and compare with the 2^{nd}-oreder-SVD model; moreover, 6) finally implement a cross-media color management system using ICC profiling strategy.

REFERENCES

1. ANSI IT8.7/3-1993, Graphic technology-Color reflection target for input scanner calibration, American National Standard Institute, Inc. (1993).

2. ANSI IT8.7/3-1993, Graphic technology-input data for characterization of 4-color printing process, American National Standard Institute, Inc. (1993).

3. Bartleson, C. J. and Grum, F, Visual Measurement, Academic Press, Inc, *Optical Radiation Measurement Volume 5, pp. 455-467* (1984).

4. Efford, N., Digital Image Processing- a practical introduction using JAVA, *pp. 133-186* (2000).

5. Hung, P. C., Colorimetric Calibration in Electronic Imaging Devices Using a Look-Up-Table Model and Interpolations, *Journal of Electronic Imaging 2(1), pp. 53-61 (January* 1993).

6. IEC 61966-2-1: 1999, Color Measurement and Management in Multimedia Systems and Equipment – Part 2-1: Default RGB Color Space – sRGB, *IEC* (1999)

7. ISO/DIS 12640-2, Graphic Technology – Prepress Digital Data Exchange – XYZ/sRGB Standard Color Image Data (XYZ/SCID), *ISO* (2000).

8. Lee, C. S., Park, Y. W., Cho, S. J., and Ha, Y. H., Gamut Mapping Algorithm Using Lightness Mapping and Multiple Anchor Points for Linear Tone and Maximum Chroma Reproduction, *Journal of Imaging Science and Technology, Volume 45, Number 3, May/June, pp. 209-223* (2001).

9. Lo, M. C., Chen, H. S., and Chueh, C. P., The Design of Advanced Gamut Mapping Algorithms in Color Management Systems, *TAGA Proceeding, pp. 15-32* (2003).

10. Lo, M. C., Chiang, R., and Shi, Lester, Color Separation for 7-ink Printing Using FM Screening, *TAGA Proceeding, pp. 716-735 (1997).*

11. Lo, M. C., Chiang, R., The Characterization Models for Multi-colored CMYKRGB, *TAGA Proceeding, pp. 242-254* (1998).

12. Luo, M. R., Xin, J. H., Rhodes, P. A., Scrivener, S. A. R., and MacDonald, L. W., Studying the performance of high resolution colour displays, *CIE 22nd SESSION-Division 1*, Melbourne, *pp. 97-100* (1991)

13. Press, W. H., Flannery, B. P. and Teukolsky, S. A., Numerical Recipes in C: The Art of Scientific Computing, 2nd ed., Cambridge University Press (1993)

14. Thurstone, L. L., A Law of Comparative Judgement, *Psychological Review*," ***34**, pp. 273-286* (1927).

15. Yule, J. A. C., Principles of Color Reproduction, *pp. 265-278* (1967).